AGU ADVANCING EARTH AND SPACE SCIENCE

Geophysical Research Letters

RESEARCH LETTER
10.1029/2020GL092166

Airborne Measurements of Contrail Ice Properties—Dependence on Temperature and Humidity

T. Bräuer[1], C. Voigt[1,2], D. Sauer[1], S. Kaufmann[1], V. Hahn[1], M. Scheibe[1], H. Schlager[1], G. S. Diskin[3], J. B. Nowak[3], J. P. DiGangi[3], F. Huber[1,4], R. H. Moore[3], and B. E. Anderson[3]

[1]German Aerospace Center, Oberpfaffenhofen, Germany, [2]Johannes Gutenberg University Mainz, Mainz, Germany, [3]NASA Langley Research Center, Hampton, VA, USA, [4]University of the Federal Armed Forces in Munich, Munich, Germany

Key Points:

- The dependence of contrail ice microphysics and extinction on ambient temperature and humidity is investigated
- Soot activation fractions in contrails formed at varying ambient temperatures are derived of soot and apparent ice emission indices
- At altitudes below 8.2 km, we observed contrails formed under incomplete soot activation near the contrail formation threshold temperature

Supporting Information:

Supporting Information may be found in the online version of this article.

Correspondence to:

T. Bräuer,
tiziana.braeuer@dlr.de

Citation:

Bräuer, T., Voigt, C., Sauer, D., Kaufmann, S., Hahn, V., Scheibe, M., et al. (2021). Airborne measurements of contrail ice properties—Dependence on temperature and humidity. *Geophysical Research Letters*, *48*, e2020GL092166. https://doi.org/10.1029/2020GL092166

Received 22 DEC 2020
Accepted 11 MAR 2021

Abstract The largest share in the climate impact of aviation results from contrail cirrus clouds. Here, the dependence of microphysical contrail ice properties and extinction on temperature and humidity is investigated. Contrail measurements were performed at various altitudes during the 2018 ECLIF II/NDMAX campaign with the NASA DC-8 chasing the DLR A320. Ice number concentrations and contrail extinction coefficients are largest at altitudes near 9.5 km, typical for short- and medium-range air traffic. At higher altitudes near 11.5 km, low ambient water vapor concentrations lead to smaller contrail particle sizes and lower extinction coefficients. In addition, contrails were detected below 8.2 km near the Schmidt-Appleman contrail formation threshold temperature. Here, only a small fraction (<15%) of the emitted soot particles were activated into ice. Our observations enhance the understanding of contrail formation near the formation threshold and give a glimpse on the altitude dependence of climate-relevant contrail properties.

Plain Language Summary Aviation has an impact on our climate and of all components, contrails are the main contributor. In January 2018, we measured contrails during the ECLIF II/NDMAX campaign. The NASA research aircraft DC-8 flew closely behind the DLR's A320. With a wide range of instruments, we measured trace gases and soot particles emitted by the A320, as well as contrail ice crystals. The data presented here are the most comprehensive contrail data set ever collected during a single flight campaign. The contrail properties are strongly influenced by ambient parameters as well as aircraft and fuel properties. Here, we focus on the influence of environmental conditions such as temperature and humidity on the formation and growth of contrail ice crystals. Therefore, we present and compare ice measurements at three different flight altitudes. For 1–2-min old contrails, we find a decrease in extinction with increasing altitude. Extinction describes the interaction between contrails and atmospheric radiation. We also find that at the lowest and warmest altitudes only a small part of the emitted soot particles is activated into contrail ice crystals. In the end, our data help to better understand contrail formation and will contribute to the research on sustainable aviation.

1. Introduction

Air traffic has contributed 3.5% to the anthropogenic climate forcing in 2011. Contrails and contrail cirrus clouds are accounted for the largest share (Brasseur et al., 2016; Burkhardt & Kärcher, 2011; Kärcher, 2016, 2018; Lee et al., 2020). A measure of climate impact is the effective radiative forcing, which is the top-of-atmosphere radiative effect induced by an anthropogenic influence, when the global surface temperature is kept constant. Lee et al. (2020) estimated a total aviation-related effective forcing for aircraft activities until 2018 of 100.9 mW m^{-2} and a contrail cirrus effective forcing under high atmospheric humidity conditions of 57.4 mW m^{-2}. Carbon dioxide emissions from aviation have a lesser climate forcing than contrail cirrus with 34.3 mW m^{-2}. As contrail cirrus clouds have much shorter lifetimes of a few days (Vázquez-Navarro et al., 2015), compared to carbon dioxide emissions with a lifetime in the atmosphere of hundreds of years, mitigation of contrail cirrus can provide a fast and effective approach to reduce aviation impact on climate.

The level of scientific understanding for contrail cirrus climate forcing is still qualified as low (Lee et al., 2020). Advanced knowledge of the contrail formation process immediately behind the aircraft is necessary to reduce uncertainties. Modern aircraft engines emit gas-phase pollutants including carbon dioxide, water vapor, nitrogen oxides, and oxidized sulfur species and also particle-phase pollutants including sulfate and organic aerosols. In addition, non-volatile, ultra-fine soot particles are produced in large quantities, typically varying between 10^{14} and 10^{16} per kilogram of fuel burned, depending on engine and fuel type (Kleine et al., 2018; Moore et al., 2017). At altitudes above 8 km and temperatures below −40°C, the hot aircraft engine exhaust is mixed with ambient air in the wake vortex and thereby cools down within seconds. The conditions in the cooling exhaust plumes are highly water super-saturated. Water vapor condenses on any available particle surface, but most favorably onto the larger soot particles (Kleine et al., 2018; Wong & Miake-Lye, 2010). Once activated, the particles become hygroscopic, continue to grow by condensation of ambient and engine-emitted water vapor and quickly undergo heterogeneous freezing to become ice particles (Heymsfield et al., 2010; Kärcher, 2018). The conditions for contrail formation are determined by the Schmidt–Appleman criterion, which defines a threshold temperature (T_{SA}) below which contrails can form (Schumann, 1996).

Flight experiments to investigate contrails have been developed and improved in the last 30 years (Schumann et al., 2017). These observations are important to reduce the uncertainties in the assessment of contrail radiative forcing (Yang et al., 2010). Because of the complexity of contrail measurements and the variety of influencing parameters, climate relevant optical parameters derived from observations are rare. One example is Gayet et al. (2002), who first presented extinction coefficients from the Fast Forward Scattering Spectrometer (FFSSP) instrument. Also, data derived during the CONCERT campaign in 2008 were used to determine a probability distribution of linear contrails extinction coefficients (Schumann et al., 2013; Voigt et al., 2011). Iwabuchi et al. (2012) studied physical and optical properties of contrails through satellite observations and derived probability distributions of the contrail optical depth in dependence of temperature, relative humidity and contrail age.

With regard to contrail modeling, Kärcher (2016) used a theoretical model to analyze contrails in their formation stage. For typical concentrations of soot particles in the modern fleet, complete activation is achieved at a temperature significantly colder than T_{SA}. The largest aerosols are preferred for activation into ice particles (Kärcher, 2018). The closer the ambient temperature is to T_{SA}, the larger the particle radii have to be for nucleation. Near T_{SA}, a fraction of unactivated soot particles remains as interstitial aerosol in the contrail (Kärcher & Yu, 2009; Kärcher et al., 2015).

The global radiative influence of contrails on a large scale is discussed by Burkhardt et al. (2018), using the global climate model ECHAM5 to show that only a few contrail cirrus outbreaks explain a large percentage of the contrail cirrus climate impact. Such outbreak situations can be effectively avoided by routing diversions of air traffic (Teoh et al., 2020). The question of how contrail formation depends on cruise altitude selections has been examined in several publications, typically using air traffic inventories and re-analysis data to assess changes in contrail coverage and fuel burn (Frömming et al., 2005; Irvine et al., 2012; Rädel & Shine, 2008). However, dependencies have not yet been investigated on the basis of airborne observations.

In this study, we discuss new contrail ice particle observations, made during the ECLIF II/NDMAX campaign. We focus on the dependence of microphysical and optical contrail properties on atmospheric conditions. This is possible because a wide range of ambient temperature and water content was measured at altitudes between 7.8 and 11.6 km.

2. Campaign and Instrumentation

2.1. The ECLIF II/NDMAX Campaign

The campaign was part of the DLR project Emission and Climate Impact of Alternative Fuels (ECLIF) and the NASA DLR Multidisciplinary Airborne Experiment (NDMAX). It was conducted in 2018 in a restricted airspace over northern Germany. The aim was to measure emissions and contrails produced by burning both standard and sustainable alternative jet fuels. The measurements were performed on board the NASA DC-8 Airborne Science Laboratory which sampled the exhaust and contrail particles behind the DLR A320 Advanced Technology Research Aircraft. The aircraft were flying in formation in an elongated, race track

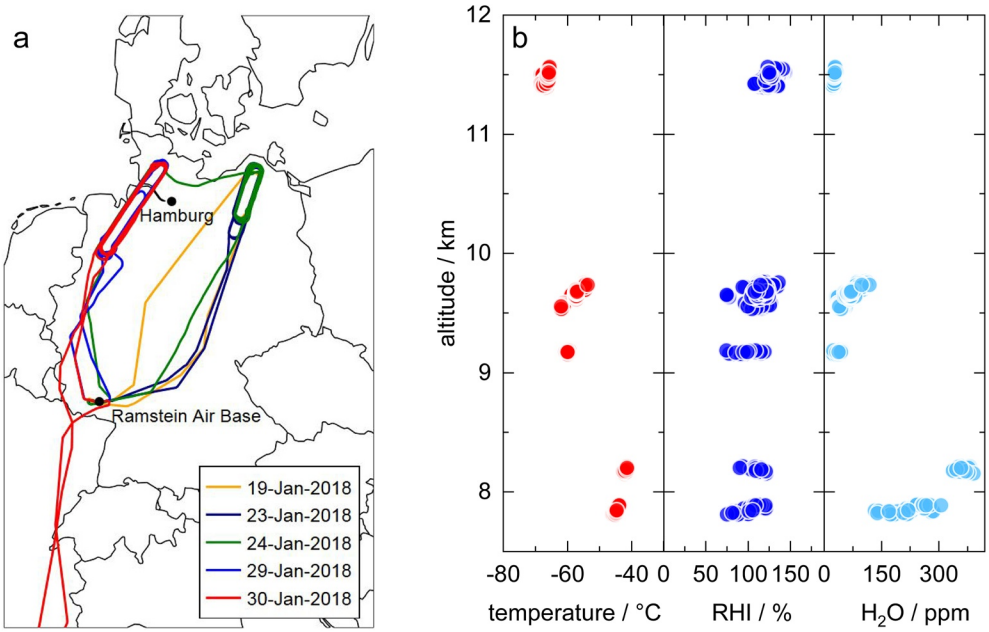

Figure 1. (a) Flight tracks over Germany are shown. The aircraft were based at the airport of the Ramstein Air Base. (b) Plume encounter mean values for ambient temperature, relative humidity with respect to ice (RHI) and water vapor (H_2O) are shown versus altitude. Measurements of five science flights on different days with varying weather conditions are included. Temperature at formation of the A320 contrail was derived of the A320 basis measuring system. RHI and H_2O were derived of the NASA DLH on board the DC-8. To transmit DC-8 measurements to the moment of formation of the A320 contrail, the data were corrected by the contrail age.

flight pattern (Figure 1a). The three fuels burned by the A320 were a reference fuel Jet A-1 and two sustainable alternative jet fuel blends SAJF 1 and SAJF 2. In total, ~2.5 h of contrails were sampled. The altitude measurement strategy entailed three flight altitudes: 7.8–8.2 km, 9.1–9.8 km and 11.4–11.6 km (pressure levels 362–343 hPa, 280–271 hPa, and 212–203 hPa). The measured age of the contrails ranged between 20 and 160 s. Because of safety reasons the distance between the aircraft had to increase at higher altitudes, so that older contrails are measured at higher altitudes and younger contrails at lower altitudes. The ambient conditions averaged over each plume encounter are shown in Figure 1b. We observe that temperature and water vapor decrease with altitude when approaching the tropopause (the transition from moist troposphere to dry stratosphere).

2.2. Particle and Trace Gas Measurements

The ice particle data were obtained with a Fast Forward Scattering Spectrometer Probe (Baumgardner et al., 1992; Brenguier et al., 1998). The instrument was mounted next to the carbon dioxide (CO_2) inlet on the upper fuselage of the DC-8, which was important to calculate CO_2-normalized ice emission indices (EI) (see Supporting Information S1). The location 3.5 m behind the aerosol inlet allows the comparison of ice and soot measurements. The probe measures particles in a diameter range between 1 and 25 μm. The particles cross the focus of an open path He–Ne laser beam with a wavelength of 632.8 nm and the forward-scattered light is measured by a photo detector. The probe was used for contrail measurements before (Chauvigné et al., 2018; Gayet et al., 2012; Jeßberger et al., 2013; Voigt et al., 2010, 2011). Its electronics received an update in 2017, such that the recording of single particles became possible. The FFSSP was size-calibrated on the basis of a T-Matrix calculation (Borrmann et al., 2000; Rosenberg et al., 2012) for an ice particle aspect ratio of 0.5 to account for nonspherical ice crystals in the young contrails. For small particles between 0.5 and 1 μm a size-dependent correction function was applied to the FFSSP data. The function is described in detail in Supporting Information S1.

Carbon dioxide is measured using a cavity ring down spectroscopy (CRDS) instrument (model G2401-m by Picarro). Sample air was passed to the CRDS instrument via a backward facing inlet, mounted to the

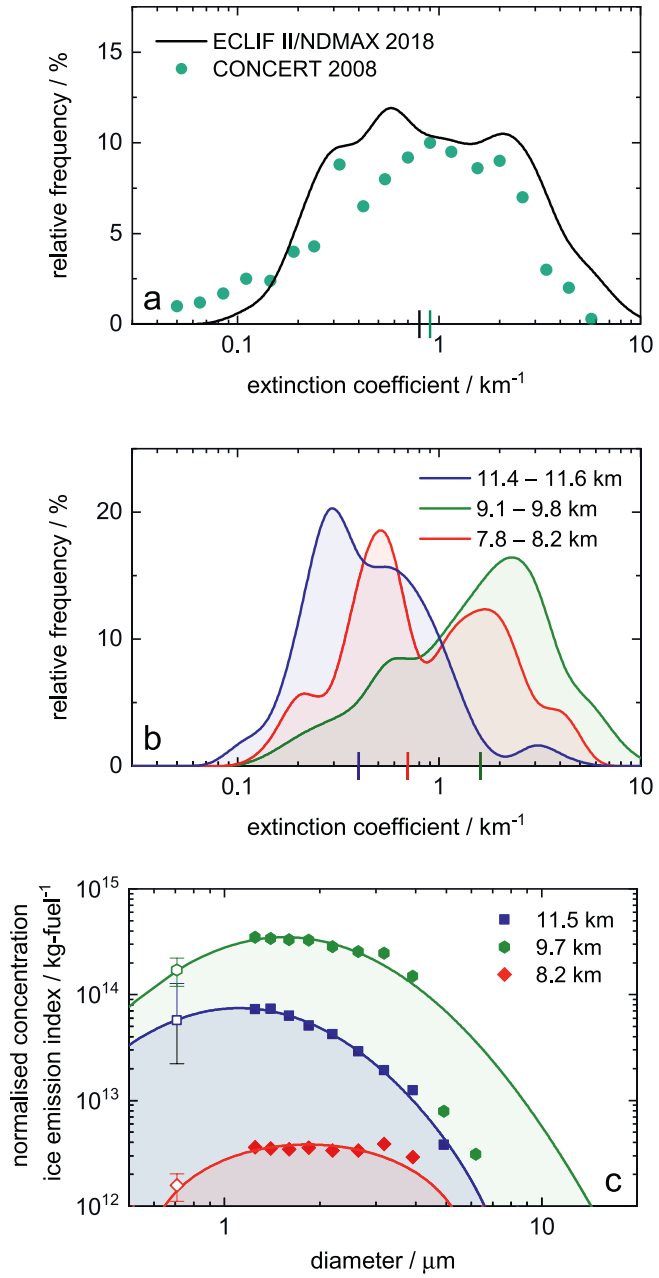

Figure 2. (a and b) Extinction coefficient probability distributions during five science flights. Lines are B-Splines fitted to the data. (a) Total extinction coefficient distributions during ECLIF II/NDMAX and CONCERT (Voigt et al., 2011) in comparison. (b) Altitude-dependent extinction coefficient distributions during ECLIF II/NDMAX. (c) Mean particle size distributions (PSD) on January 24, 2018. Lines show the log-normal fit. Hollow symbols show concentrations for diameters between 0.5 and 1 µm estimated by a correction factor (see Supporting Information S1).

fuselage of the DC-8 near the FFSSP. A near-infrared laser emits pulses into a three-mirror cavity. Here, the sample gas is circulated with an effective path length of about 20 km. The time required to attenuate the laser pluses in the cavity is proportional to the mole fraction of CO_2 in the sample air. The effect of water vapor on the CO_2 reading is corrected during post-processing (Rella et al., 2013). The time resolution of the carbon dioxide data from the CRDS instrument is nominally 1 Hz. But the CO_2 signal rise time (10%–90%) and fall time (90%–10%) is 1.5 s. Therefore, averaging times may exceed the time resolution and the measurement interval of the CO_2 measurements is up to 2 s. The precision is 0.05 ppmv for 2 s of data recordings and the accuracy is 0.3 ppmv.

Soot particle concentrations are measured as the number concentrations of non-volatile particulate matter (nvPM) by a condensation particle counter. The instrument is based on the model 3010 by TSI, modified and optimized for airborne application. Particles were sampled through a forward-facing aerosol inlet. The inlet was not isokinetic, but designed in a way that contrail ice particles are expected to completely evaporate in the shock-front generated by the inlet. In the thermodenuder, the particles are heated to 250°C in order to evaporate volatile components, so that only the non-volatile aerosol components remain. They are assumed to be predominantly composed of soot particles. The data have been corrected for reduced detection efficiencies in low pressure environments (Noone & Hansson, 1990) and particle losses in the thermodenuder.

Water vapor was measured by the NASA Langley Diode Laser Hygrometer (DLH), an open-path infrared absorption instrument with a long history of measurements on the DC-8 and many other airborne platforms (Diskin et al., 2002; Podolske et al., 2003). The DLH operates on one of three absorption lines in the near-infrared around 1.395 µm, switching quickly and automatically between lines as conditions change, and measures at a rate of 20 Hz.

3. Contrail Parameters at Varying Ambient Conditions

The optical thickness of a contrail is an important quantity for its individual impact on the transport of radiation through the atmosphere. Contributing parameters are the geometrical thickness of the contrail, its ice mass concentration and the extinction properties of the ice crystals. For this reason, the ice extinction coefficient is calculated for ECLIF II/NDMAX contrail measurements by summing the projected area of the particles, the number concentration and extinction efficiencies (Schumann et al., 2011). The extinction efficiencies were calculated for a wavelength of 550 nm and approach a value of 2 for large ice particles.

Figure 2a shows a probability distribution of ECLIF II/NDMAX extinction coefficients calculated from all FFSSP ice particle measurements. The measurements are compared to results from the 2008 CONCERT campaign (Jeßberger et al., 2013; Voigt et al., 2010, 2011). During CONCERT, contrails of different aircraft types were sampled; for example, A319, A340, and A380. Median extinction coefficients for both missions are depicted as colored ticks on the logarithmic *x*-axis. For ECLIF II/NDMAX the total extinction coefficient median was 0.8 km^{-1} and for CONCERT the total extinction coefficient median was 0.9 km^{-1}. Thus the medians and distributions are in the same range.

Table 1
Measurement Conditions and Properties on January 24, 2018

alt / km mean	p / hPa mean	t / s sum	T / °C mean	RHI / % range	H_2O / ppm range	age / s range	d_{eff} / µm mean	N_{ice} / cm^{-3} max	b_{ext} / km^{-1} median
11.5	208.7	1419	−67.7	120–143	21–30	97–152	2.3	219	0.4
9.7	275.3	1348	−54.8	93–136	83–118	46–145	2.7	1306	2.4
8.2	344.2	988	−41.8	90–121	337–390	28–81	3.0	188	0.5

Abbreviations: age, contrail age; alt, altitude; b_{ext}, extinction coefficient; d_{eff}, effective diameter; H_2O, water vapor; N_{ice}, ice number concentration; p, pressure level; RHI, relative humidity with respect to ice; T, ambient temperature; t, sample time.

Figure 2b shows how the extinction coefficient probability distributions vary with the altitude. Median extinction coefficients were 0.4 km^{-1} for altitudes above 11.4 km, 0.7 km^{-1} for altitudes below 8.2 km and 1.6 km^{-1} for altitudes 9.1–9.8 km.

To investigate factors that control extinction coefficient distributions, we examine altitude-dependent particle size distributions (PSD) on January 24, 2018 shown in Figure 2c. We compare PSDs for a single day and for the same fuel, to avoid distortions due to variation in tropopause positions and fuel aromatic content. The PSDs are dilution-normalized to account for effects of dilution, contrail age and spatial inhomogeneities on the ice number concentration. Concentrations for diameters between 0.5 and 1 µm in the PSDs are derived by a correction factor (see Supporting Information S1). The relative errors for these small particle estimations depend on the effective diameter and are 30% for low and medium altitudes and further increasing for high altitudes. Table 1 lists the measurement conditions and properties for the flight on January 24, 2018, complementing Figure 2c. In the following, the differences in the extinction and the PSD of the three altitudes are explained based on the mechanisms of contrail formation and growth.

On January 24, 2018, the particle concentrations at altitudes between 9.1 and 9.8 km were highest with maximum number densities of 1,250 cm^{-3}. The ambient conditions here were favorable for contrail formation (−50°C to −60°C and up to 140% RHI) and support the theory of an extensive activation of nvPM. High ice number concentrations at this flight altitude consequently lead to increased extinction coefficients. Thus, based on ECLIF II/NDMAX observations, we conclude that the instantaneous impact of young contrails on the atmospheric radiation is largest at these altitudes, which are typical for short and medium range flights. The mean age for contrails encountered at this flight altitude on January 24, 2018 was 115 s with a mean effective diameter of 2.7 µm. In persistent contrail conditions, effective diameters grow with age, but the ice number concentrations decrease due to sedimentation and subsequent sublimation effects (Kleine et al., 2018; Kärcher et al., 2018).

In contrast to the medium flight level, the contrails formed above 11.4 km exhibited the lowest median extinction coefficient. These altitudes are typically reached by transatlantic air traffic in regions with a high probability for contrail outbreaks. Mean contrail age was 140 s and both the mean effective diameter and maximum number concentrations were small with 2.3 µm and 220 cm^{-3}, respectively. The low number concentrations are interesting, because the low temperature range (−60°C to −70°C) and supersaturation with respect to ice should have produced high activation of nvPM. In spite of frequent supersaturation, the absolute humidity was low at these high altitudes with less than 40 ppm of water vapor (H_2O) measured at contrail formation compared to 50–100 ppm at medium flight altitudes. In conclusion, the reduced available H_2O at low ambient pressures between 272 and 280 hPa led to a reduced growth and size of ice particles. Therefore, it is possible that ice particles were smaller than the FFSSP detection limit of 0.5 µm at these higher altitudes and that a certain amount of particles was not measured. The correction factor for ice particles between 0.5 and 1 µm gives an increase of up to 10% for the ice number concentrations at high altitudes. This increase represents a lower limit, as the maximum of the particle size distribution is shifted toward the FFSSP lower detection threshold. The impact of such small ice particles on extinction, however, is low.

Finally, at flight altitudes below 8.2 km the ice particle concentrations were also reduced (maximum 185 cm^{-3}). This can be explained by the relatively high temperatures close to −40°C and broad range of RHI (90–120%). The ambient conditions caused a reduced activation of nvPM here. The mean contrail age was

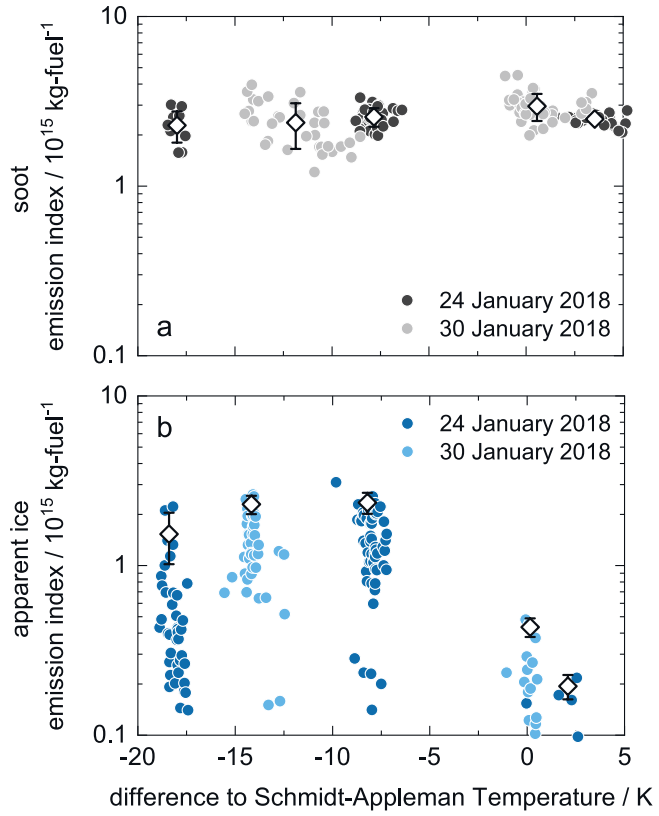

Figure 3. Emission indices (EI) versus the difference dT_{SA} between ambient temperature and Schmidt–Appleman temperature are shown. (a) Non-volatile particulate matter (nvPM) EI EI_{nvPM}. Diamonds show the mean values. (b) Apparent ice. Diamonds show the mean upper 15%.

42 s, as safety regulations made it possible to fly relatively close behind the A320 at this flight altitude. The abundance of H_2O with mixing ratios up to 400 ppm explain the high effective mean diameter of 3.0 μm at this flight altitude, as more H_2O is available for the growth of a reduced number of particles. The combination of large but fewer ice particles leads to a low median extinction coefficient of 0.5 km^{-1}. This value is comparable with the extinction level at the highest altitudes.

In summary, this detailed analysis demonstrates that young contrail optical extinction strongly depends on the formation and early growth mechanisms at the varying altitudes. The further development and life-cycle depend not only on meteorological parameters like temperature and humidity, but vertical wind shear, atmospheric stability, the depth of the supersaturated layer in which the contrails are formed and also the radiation scenario plays a role in the further evolution of the contrail (Unterstrasser et al., 2017). For ECLIF II/NDMAX conditions during winter time and in mid-latitudes, initial extinction was highest at the medium flight altitudes between 9.1 and 9.8 km. It was reduced at lower and therefore warmer flight altitudes below 8.2 km and smallest at the highest and therefore drier altitudes above 11.4 km.

4. Soot and Ice EI in Dependence of the Temperature

The difference dT_{SA} between the ambient temperature and the Schmidt–Appleman temperature, which typically increases with altitude, is a driving factor for the activation of plume particles (Kärcher, 2018). For calculation of the Schmidt–Appleman temperature please see Supporting Information S1. In Figure 3, the EI of nvPM and ice versus the difference dT_{SA} are presented. The data are limited to SAJF 1 to avoid distortions due to variation in fuel aromatic content. Therefore, measurements of the flights of January 24 and 30, 2018 are depicted. For the calculation of the Schmidt–Appleman temperature, an overall propulsion efficiency of 0.31 was chosen as a most conservative estimate. EI_{nvPM} increase slightly at low flight altitudes due to increased fuel flows on levels of higher atmospheric pressure and range between 1.2 and 4.5×10^{15} kg-$fuel^{-1}$. The activation of nvPM into ice particles can be calculated within the measuring range by comparing the determined EI of nvPM and ice. To account for sublimation effects, we adapt Kleine et al. (2018) and use only the mean of the upper 15% of ice EI. In addition, all contrails developed and observed in sub-saturated conditions are excluded. For dT_{SA} between −16 and −6.9 K, at flight altitudes between 9.5 and 9.8 km, the activation is nearly complete with 91.7%–97%.

Between −18.9 and −17.4 K, in the coldest conditions above flight altitudes of 11.5 km, apparent ice EI are reduced. As explained above, we expect full soot activation due to the favorable conditions at these altitudes. Therefore, we can comprehend that about 30% of ice particles were not detected or not accounted for at the higher altitude due to size.

The contrail data are also used to evaluate near-threshold conditions, where only the most soluble and large particles are water activated and grow into detectable ice particles (Kärcher, 2018; Kärcher & Yu, 2009; Kärcher et al., 2015). In the near-threshold conditions the measured AEI_{ice} are strongly reduced. For dT_{SA} between −1.1 and 1.1 K on January 30, 2018 an activation of 14.7% can be determined. On January 24, 2018, the calculated activation is 7.8% for dT_{SA} between 0 and 3.0 K. Interestingly, for both flights, positive dT_{SA} values were calculated for the lowest flight altitudes. On January 30, 2018, dT_{SA} was maximum 1.1 K at flight altitudes below 7.9 km, and on January 24, 2018, dT_{SA} was maximum 3.0 K at flight altitudes below 8.2 km. On both days, contrails seem to have formed in conditions warmer than the Schmidt–Appleman threshold temperature. Similar situations were observed before (Gayet et al., 1996; Jensen et al., 1998) and possible explanations are discussed in Schumann et al. (2017). One explanation for positive dT_{SA} can be

instrument and measurement uncertainties. Instrument uncertainties for the calculation of temperature differences at low altitudes are ±1.9 K. Also, measurements of contrails that presumably formed at temperatures exceeding the Schmidt–Appleman temperature may be explained by atmospheric variability and mixing in the exhaust. This can lead to non-equilibrium processes, which are not reflected by the Schmidt–Appleman criterion. The possibility that the observed contrails are not exhaust contrails but aerodynamic contrails, which result from the cooling effect of accelerated flow over aircraft wings (Gierens et al., 2009), can be ruled out because the measured particle sizes exceed typical PSDs of aerodynamic contrails (Gierens et al., 2011).

In summary, we show that dT_{SA} can be an indicator of the nvPM activation fraction. The activation is reduced with the ambient temperature approaching the formation threshold temperature. Also, reduced ice EI were estimated for high temperature differences and are justified to some extent with the lack of available background water vapor and the instrument detection limit.

5. Conclusions and Outlook

Microphysical contrail properties and extinction coefficients measured behind an A320 are of similar magnitude as observed previously (Schumann et al., 2017; Voigt et al., 2010), but observations during ECLIF II/NDMAX offer a more extensive data set than previous campaigns. It is demonstrated how differences in temperature, RHI and H_2O influence ice number concentration and particle size and in turn, the extinction of young contrails. We show that extinction of contrails at an age of one to two minutes is maximum within an altitude band in the mid troposphere.

The activation of nvPM is of special interest. Activation is incomplete at lower altitudes and for temperatures close to the Schmidt–Appleman temperature. By analyzing the dependence of aerosol activation efficiency on ambient parameters, conditions close to formation threshold can be used for model validation in the future. For upcoming campaigns, we recommend that RHI be measured on board the source aircraft for a more accurate determination of the contrail formation conditions. For determination of ice EI, for example when comparing different fuel or engine types, not only sublimation effects but also ambient conditions and their influence on activation of nvPM have to be considered.

Data Availability Statement

The data are available at https://science-data.larc.nasa.gov/aero-fp/projects/.

Acknowledgments
T. Bruer. and C. Voigt. acknowledge funding by the Helmholtz Association under contract W2/W3-60. C. V. acknowledges funding by the German Research Foundation for SPP HALO 1294 and project VO 1504/7-1. We thank our colleagues at the German Aerospace Center in Oberpfaffenhofen: Yvonne Boose, Manuel Moser, Marina Schimpf, Tina Jurkat-Witschas, and Christopher Heckl for excellent measurement operations, Klaus Gierens for his constructive inputs concerning aerodynamic contrails and Ulrich Schumann for his estimate of the overall propulsion efficiency of the A320. Open access funding enabled and organized by Projekt DEAL.

References

Baumgardner, D., Dye, J. E., & Gandrud, B. W. (1992). Interpretation of measurements made by the forward scattering spectrometer probe (FSSP-300) during the airborne Artic stratosheric expedition. *Journal of Geophysical Research*, *97*, 8035–8046. https://doi.org/10.21236/ada249893

Borrmann, S., Luo, B., & Mishchenko, M. (2000). Application of the t-matrix method to the measurement of aspherical (ellipsoidal) particles with forward scattering optical particle counters. *Journal of Aerosol Science*, *31*, 789–799. https://doi.org/10.1016/s0021-8502(99)00563-7

Brasseur, G. P., Gupta, M., Anderson, B. E., Balasubramanian, S., Barrett, S., Duda, D., et al. (2016). Impact of aviation on climate: FAA's aviation climate change research initiative (ACCRI) phase II. *Bulletin of the American Meteorological Society*, *97*(4), 561–583. https://doi.org/10.1175/BAMS-D-13-00089.1

Brenguier, J.-L., Bourrianne, T., Coelho, A., Isbert, J., Peytavi, R., Trevarin, D., & Weschler, P. (1998). Improvements of droplet size distribution measurements with the fast-FSSP (forward scattering spectrometer probe). *Journal of Atmospheric and Oceanic Technology*, *15*, 1077–1090. https://doi.org/10.1175/1520-0426(1998)015⟨1077:IODSDM⟩2.0.co;2

Burkhardt, U., Bock, L., & Bier, A. (2018). Mitigating the contrail cirrus climate impact by reducing aircraft soot number emissions. *NPJ Climate and Atmospheric Science*, *1*(1), 1–7. https://doi.org/10.1038/s41612-018-0046-4

Burkhardt, U., & Kärcher, B. (2011). Global radiative forcing from contrail cirrus. *Nature Climate Change*, *1*, 54–58. https://doi.org/10.1038/nclimate1068

Chauvigné, A., Jourdan, O., Schwarzenboeck, A., Gourbeyre, C., Gayet, J. F., Voigt, C., et al. (2018). Statistical analysis of contrail to cirrus evolution during the contrail and cirrus experiment (concert). *Atmospheric Chemistry and Physics*, *18*(13), 9803–9822. https://doi.org/10.5194/acp-18-9803-2018

Diskin, G. S., Podolske, J. R., Sachse, G. W., & Slate, T. A. (2002). Open-path airborne tunable diode laser hygrometer. In A. Fried (Ed.), *Diode lasers and applications in atmospheric sensing* (Vol. 4817, pp. 196–204). SPIE. https://doi.org/10.1117/12.453736

Frömming, C., Marquart, S., Sausen, R., & Lee, D. (2005). The impact of cruise altitude on contrails and related radiative forcing. *Meteorologische Zeitschrift*, *14*, 563–572. https://doi.org/10.1127/0941-2948/2005/0048

Gayet, J.-F., Auriol, F., Minikin, A., Ström, J., Seifert, M., Krejci, R., et al. (2002). Quantitative measurement of the microphysical and optical properties of cirrus clouds with four different in situ probes: Evidence of small ice crystals. *Geophysical Research Letters*, *29*(24). https://doi.org/10.1029/2001GL014342

Gayet, J.-F., Febvre, G., Brogniez, G., Chepfer, H., Renger, W., & Wendling, P. (1996). Microphysical and optical properties of cirrus and contrails: Cloud field study on 13 October 1989. *Journal of the Atmospheric Sciences*, *53*(1), 126–138. https://doi.org/10.1175/1520-0469(1996)053⟨0126:MAOPOC⟩2.0.CO;2

Gayet, J.-F., Shcherbakov, V., Voigt, C., Schumann, U., Schäuble, D., Jeßberger, P., et al. (2012). The evolution of microphysical and optical properties of an A380 contrail in the vortex phase. *Atmospheric Chemistry and Physics*, *12*, 6629–6643. https://doi.org/10.5194/acp-12-6629-2012

Gierens, K., Ästner, M. K., & Klatt, D. K. (2011). Iridescent aerodynamic contrails: The norderney case of 27 June 2008. *Meteorologische Zeitschrift*, *20*(3), 305–311. https://doi.org/10.1127/0941-2948/2011/0497

Gierens, K., Kärcher, B., Mannstein, H., & Mayer, B. (2009). Aerodynamic contrails: Phenomenology and flow physics. *Journal of the Atmospheric Sciences*, *66*(2), 217–226. https://doi.org/10.1175/2008JAS2767.1

Heymsfield, A., Baumgardner, D., DeMott, P., Forster, P., Gierens, K., & Kärcher, B. (2010). Contrail microphysics. *Bulletin of the American Meteorological Society*, *91*, 465–472. https://doi.org/10.1175/2009BAMS2839.1

Irvine, E. A., Hoskins, B. J., & Shine, K. P. (2012). The dependence of contrail formation on the weather pattern and altitude in the north Atlantic. *Geophysical Research Letters*, *39*, L12802. https://doi.org/10.1029/2012GL051909

Iwabuchi, H., Yang, P., Liou, K. N., & Minnis, P. (2012). Physical and optical properties of persistent contrails: Climatology and interpretation. *Journal of Geophysical Research*, *117*, D06215. https://doi.org/10.1029/2011jd017020

Jeßberger, P., Voigt, C., Schumann, U., Sölch, I., Schlager, H., Kaufmann, S., et al. (2013). Aircraft type influence on contrail properties. *Atmospheric Chemistry and Physics*, *13*, 11965–11984. https://doi.org/10.5194/acp-13-11965-2013

Jensen, E. J., Toon, O. B., Kinne, S., Sachse, G. W., Anderson, B. E., Chan, K. R., et al. (1998). Environmental conditions required for contrail formation and persistence. *Journal of Geophysical Research*, *103*, 3929–3936. https://doi.org/10.1029/97jd02808

Kärcher, B. (2016). The importance of contrail ice formation for mitigating the climate impact of aviation. *Journal of Geophysical Research: Atmospheres*, *121*, 3497–3505. https://doi.org/10.1002/2015JD024696

Kärcher, B. (2018). Formation and radiative forcing of contrail cirrus. *Nature Communications*, *9*, 1–17. https://doi.org/10.1038/s41467-018-04068-0

Kärcher, B., Burkhardt, U., Bier, A., Bock, L., & Ford, I. J. (2015). The microphysical pathway to contrail formation. *Journal of Geophysical Research: Atmospheres*, *120*, 7893–7927. https://doi.org/10.1002/2015jd023491

Kärcher, B., Kleine, J., Sauer, D., & Voigt, C. (2018). Contrail formation: Analysis of sublimation mechanisms. *Geophysical Research Letters*, *45*, 13547–13552. https://doi.org/10.1029/2018GL079391

Kärcher, B., & Yu, F. (2009). Role of aircraft soot emissions in contrail formation. *Geophysical Research Letters*, *36*, 1–5. https://doi.org/10.1029/2008GL036649

Kleine, J., Voigt, C., Sauer, D., Schlager, H., Scheibe, M., Jurkat-Witschas, T., et al. (2018). In situ observations of ice particle losses in a young persistent contrail. *Geophysical Research Letters*, *45*, 13553–13561. https://doi.org/10.1029/2018GL079390

Lee, D. S., Fahey, D. W., Skowron, A., Allen, M. R., Burkhardt, U., Chen, Q., et al. (2021). The contribution of global aviation to anthropogenic climate forcing for 2000 to 2018. *Atmospheric Environment*, *244*, 117834. https://doi.org/10.1016/j.atmosenv.2020.117834

Moore, R. H., Thornhill, K. L., Weinzierl, B., Sauer, D., D'Ascoli, E., Kim, J., et al. (2017). Biofuel blending reduces particle emissions from aircraft engines at cruise conditions. *Nature*, *543*, 411–415. https://doi.org/10.1038/nature21420

Noone, K. J., & Hansson, H.-C. (1990). Calibration of the TSI 3760 condensation nucleus counter for nonstandard operating conditions. *Aerosol Science and Technology*, *13*(4), 478–485. https://doi.org/10.1080/02786829008959462

Podolske, J. R., Sachse, G. W., & Diskin, G. S. (2003). Calibration and data retrieval algorithms for the NASA Langley/Ames diode laser hygrometer for the NASA transport and chemical evolution over the pacific (TRACE-P) mission. *Journal of Geophysical Research*, *108*(D20), 8792. https://doi.org/10.1029/2002JD003156

Rädel, G., & Shine, K. P. (2008). Radiative forcing by persistent contrails and its dependence on cruise altitudes. *Journal of Geophysical Research*, *113*, D07105. https://doi.org/10.1029/2007JD009117

Rella, C. W., Chen, H., Andrews, A. E., Filges, A., Gerbig, C., Hatakka, J., et al. (2013). High accuracy measurements of dry mole fractions of carbon dioxide and methane in humid air. *Atmospheric Measurement Techniques*, *6*(3), 837–860. https://doi.org/10.5194/amt-6-837-2013

Rosenberg, P. D., Dean, A. R., Williams, P. I., Dorsey, J. R., Minikin, A., Pickering, M. A., & Petzold, A. (2012). Particle sizing calibration with refractive index correction for light scattering optical particle counters and impacts upon PCASP and CDP data collected during the fennec campaign. *Atmospheric Measurement Techniques*, *5*(5), 1147–1163. https://doi.org/10.5194/amt-5-1147-2012

Schumann, U. (1996). Über Bedingungen zur Bildung von Kondensstreifen aus Flugzeugabgasen. *Meteorologische Zeitschrift*, *5*, 4–23. https://doi.org/10.1127/metz/5/1996/4

Schumann, U., Baumann, R., Baumgardner, D., Bedka, S. T., Duda, D. P., Freudenthaler, V., et al. (2017). Properties of individual contrails: A compilation of observations and some comparisons. *Atmospheric Chemistry and Physics*, *17*(1), 403–438. https://doi.org/10.5194/acp-17-403-2017

Schumann, U., Jeßberger, P., & Voigt, C. (2013). Contrail ice particles in aircraft wakes and their climatic importance. *Geophysical Research Letters*, *40*, 2867–2872. https://doi.org/10.1002/grl.50539

Schumann, U., Mayer, B., Gierens, K., Unterstrasser, S., Jessberger, P., Petzold, A., et al. (2011). Effective radius of ice particles in cirrus and contrails. *Journal of the Atmospheric Sciences*, *68*(2), 300–321. https://doi.org/10.1175/2010JAS3562.1

Teoh, R., Schumann, U., Majumdar, A., & Stettler, M. E. J. (2020). Mitigating the climate forcing of aircraft contrails by small-scale diversions and technology adoption. *Environmental Science & Technology*, *54*(5), 2941–2950.(PMID: 32048502). https://doi.org/10.1021/acs.est.9b05608

Unterstrasser, S., Gierens, K., Sölch, I., & Lainer, M. (2017). Numerical simulations of homogeneously nucleated natural cirrus and contrail-cirrus. Part 1: How different are they? *Meteorologische Zeitschrift*, *26*(6), 621–642. https://doi.org/10.1127/metz/2016/0777

Vázquez-Navarro, M., Mannstein, H., & Kox, S. (2015). Contrail life cycle and properties from 1 year of MSG/SEVIRI rapid-scan images. *Atmospheric Chemistry and Physics*, *15*(15), 8739–8749. https://doi.org/10.5194/acp-15-8739-2015

Voigt, C., Schumann, U., Jeßberger, P., Jurkat, T., Petzold, A., Gayet, J.-F., et al. (2011). Extinction and optical depth of contrails. *Geophysical Research Letters*, *38*, L11806. https://doi.org/10.1029/2011GL047189

Voigt, C., Schumann, U., Jurkat, T., Schäuble, D., Schlager, H., Petzold, A., et al. (2010). In-situ observations of young contrails - Overview and selected results from the CONCERT campaign. *Atmospheric Chemistry and Physics Discussions*, *10*, 9039–9056. https://doi.org/10.5194/acpd-10-12713-2010

Wong, H.-W., & Miake-Lye, R. C. (2010). Parametric studies of contrail ice particle formation in jet regime using microphysical parcel modeling. *Atmospheric Chemistry and Physics*, *10*(7), 3261–3272. https://doi.org/10.5194/acp-10-3261-2010

Yang, P., Hong, G., Dessler, A. E., Ou, S. S. C., Liou, K.-N., Minnis, P., & Harshvardhan (2010). Contrails and induced cirrus. *Bulletin of the American Meteorological Society*, *91*(4), 473–478. https://doi.org/10.1175/2009BAMS2837.1

References From the Supporting Information

Francis, P. N., Jones, A., Saunders, R. W., Shine, K. P., Slingo, A., & Sun, Z. (1994). An observational and theoretical study of the radiative properties of cirrus: Some results from ICE'89. *Quarterly Journal of the Royal Meteorological Society*, *120*, 809–848. https://doi.org/10.1002/qj.49712051804

Poll, D. I. A., & Schumann, U. (2020). An estimation method for the fuel burn and other performance characteristics of civil transport aircraft in the cruise. Part 1 fundamental quantities and governing relations for a general atmosphere. *Aeronautical Journal*, *125*, 257–295. https://doi.org/10.1017/aer.2020.62